Article

Cell Reports

Splicing and Chromatin Factors Jointly Regulate Epidermal Differentiation

Graphical Abstract

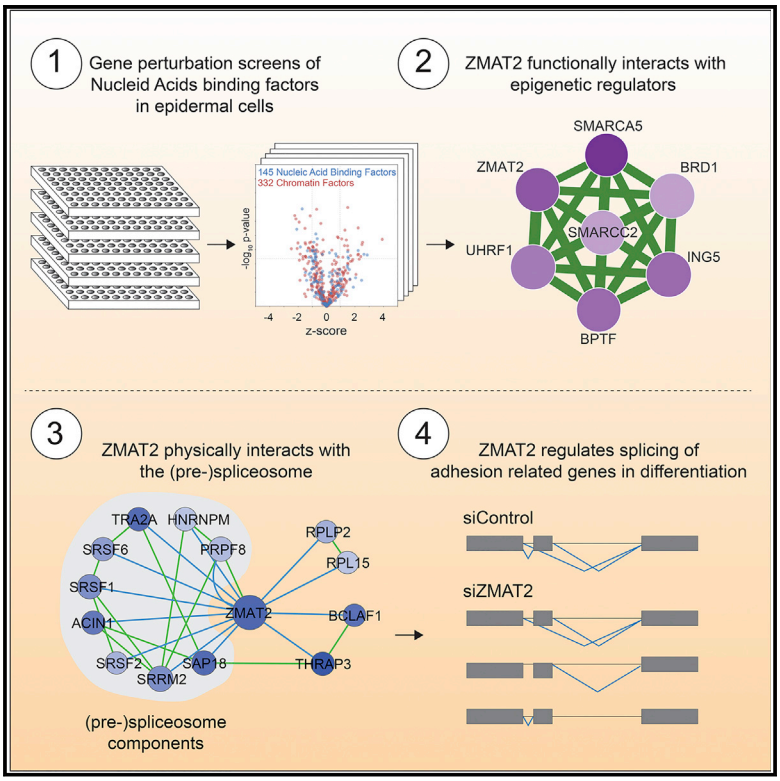

Highlights

- Gene perturbation screens identify a role for ZMAT2 in human epidermal differentiation
- ZMAT2 functionally interacts with chromatin regulators in epidermal differentiation
- ZMAT2 interacts with the pre-spliceosome and a specific subset of RNA transcripts
- ZMAT2 regulates splicing of differentiation and adhesion-associated transcripts

Authors

Sabine E.J. Tanis, Pascal W.T.C. Jansen, Huiqing Zhou, Simon J. van Heeringen, Michiel Vermeulen, Markus Kretz, Klaas W. Mulder

Correspondence

k.mulder@science.ru.nl

In Brief

Tanis et al. use gene perturbation screens and multiple -omics approaches to identify ZMAT2 as a regulator of epidermal differentiation. Moreover, ZMAT2 works in conjunction with several chromatin modifiers to control genes involved in cell adhesion processes.

Tanis et al., 2018, Cell Reports *25*, 1292–1303
October 30, 2018
https://doi.org/10.1016/j.celrep.2018.10.017

CellPress

OPEN ACCESS
CellPress

Cell Reports
Article

Splicing and Chromatin Factors Jointly Regulate Epidermal Differentiation

Sabine E.J. Tanis,[1,2] Pascal W.T.C. Jansen,[1,3,4] Huiqing Zhou,[1,2,5] Simon J. van Heeringen,[1,2] Michiel Vermeulen,[1,3,4] Markus Kretz,[6] and Klaas W. Mulder[1,2,7,*]

[1]Faculty of Science, Radboud University, Nijmegen, the Netherlands
[2]Department of Molecular Developmental Biology, Radboud Institute for Molecular Life Sciences, Nijmegen, the Netherlands
[3]Department of Molecular Biology, Radboud Institute for Molecular Life Sciences, Nijmegen, the Netherlands
[4]Oncode Institute, Nijmegen, the Netherlands
[5]Department of Human Genetics, Radboud University Medical Center, Nijmegen, the Netherlands
[6]Faculty of Biology and Preclinical Medicine, Institute for Biochemistry, Genetics, and Microbiology, University of Regensburg, Regensburg, Germany
[7]Lead Contact
*Correspondence: k.mulder@science.ru.nl
https://doi.org/10.1016/j.celrep.2018.10.017

SUMMARY

Epidermal homeostasis requires balanced progenitor cell proliferation and loss of differentiated cells from the epidermal surface. During this process, cells undergo major changes in their transcriptional programs to accommodate new cellular functions. We found that transcriptional and post-transcriptional mechanisms underlying these changes jointly control genes involved in cell adhesion, a key process in epidermal maintenance. Using siRNA-based perturbation screens, we identified DNA and/or RNA binding regulators of epidermal differentiation. Computational modeling and experimental validation identified functional interactions between the matrin-type 2 zinc-finger protein ZMAT2 and the epigenetic modifiers ING5, SMARCA5, BRD1, UHRF1, BPTF, and SMARCC2. ZMAT2 is an interactor of the pre-spliceosome that is required to keep cells in an undifferentiated, proliferative state. RNA immunoprecipitation and transcriptome-wide RNA splicing analysis showed that ZMAT2 associates with and regulates transcripts involved in cell adhesion in conjunction with ING5. Thus, joint control by splicing regulation, histone, and DNA modification is important to maintain epidermal cells in an undifferentiated state.

INTRODUCTION

As our understanding of gene expression regulation improves, so does our awareness of its complex dynamics and timing. The transcription machinery and its co-factors, chromatin state, RNA splicing, and microRNAs (miRNAs) are only some of the myriad of processes contributing to the versatile functions of a cell. Regulation of gene expression is of particular importance for governing the delicate balance between proliferation and differentiation in stratified epithelial tissues such as the skin, breast, or intestine. The high renewal rate in these tissues requires tight regulation of gene expression programs to avoid the generation of aberrantly behaving cells giving rise to diseases. Here, we use primary human keratinocytes as a model to study the regulation of gene expression programs governing epidermal proliferation and differentiation. The epidermal layer of the skin is completely replenished each month in a process driven by epidermal stem cells (keratinocytes), which reside attached on the basal membrane. Upon initiation of differentiation, these cells stop proliferating, release their integrin anchors, and move through the different layers of the skin, traveling upward through the spinous and the granular layers (Moreno-Layseca and Streuli, 2014). Eventually, they end up denucleated and heavily interconnected in the cornified layer, where they are shed from the surface. This process is marked by, among others, downregulation of integrins and upregulation of differentiation genes such as envoplakin (ENV), periplakin (PPL) (Ruhrberg et al., 1997), involucrin (INV), and transglutaminase 1 (TGM1) (Eckert et al., 2005). Throughout this transition they continuously change and fine-tune their expression programs using transcriptional and post-transcriptional processes in a differentiation state-dependent manner.

These transitions in gene expression programs are controlled by regulatory mechanisms provided by epigenetic factors, transcription factors, and post-transcriptional processes such as splicing. Epigenetic factors regulate chromatin accessibility through remodeling (BPTF, SMARCA5) or by adding or removing histone or DNA modifications (ING5, UHRF1) (Mulder et al., 2012). Open chromatin structures allow for transcription factors to bind their motifs and enable activation of gene expression programs. There are several transcription factors that have a known role in keratinocyte biology (AP1, ETS family [Eckert et al., 1997; Nagarajan et al., 2010]) to regulate the expression of differentiation markers (e.g., IRF6 [Biggs et al., 2012; Botti et al., 2011] and MAFB [Miyai et al., 2016]). The emerging RNA transcript is then found by RNA-binding proteins that edit and protect it on its way to being translated into a protein. One of the most important RNA editing processes is RNA splicing, in which introns are excised from the immature transcript, generating a mature RNA transcript. More extensive editing via alternative splicing

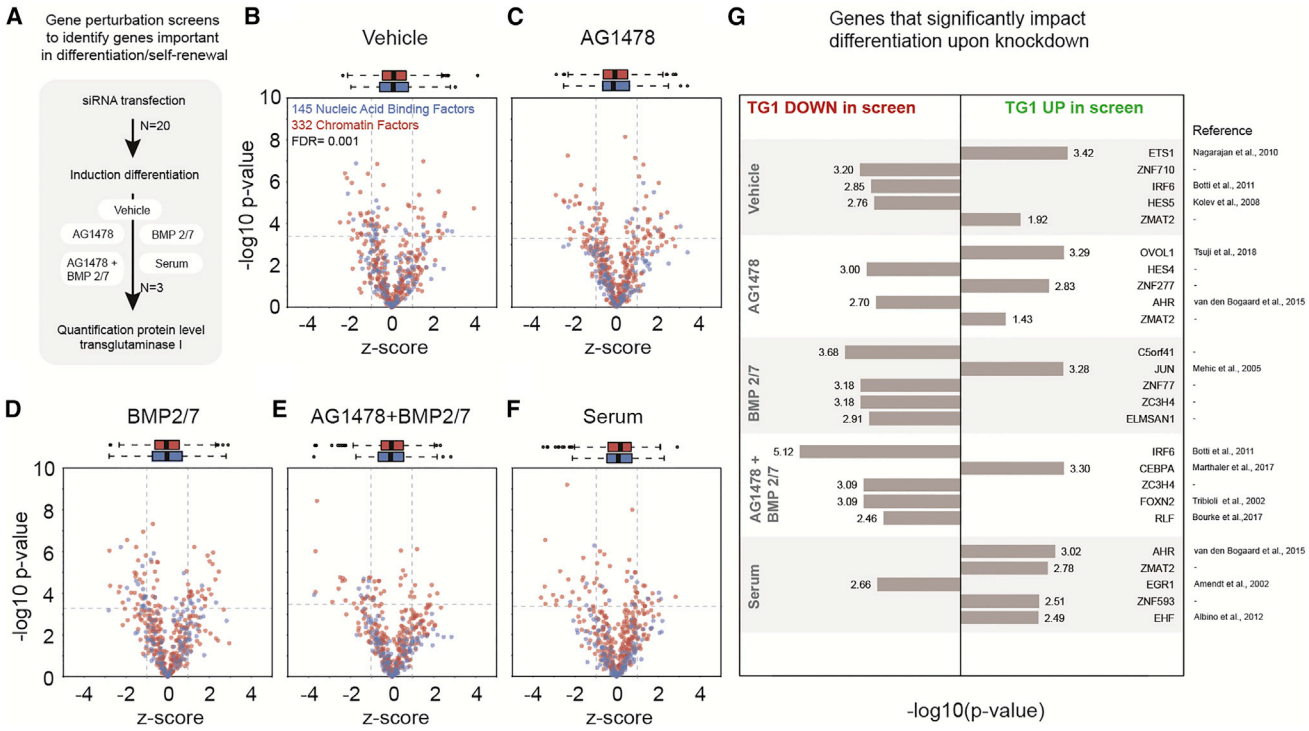

Figure 1. Gene Perturbation Screens Reveal Nucleic Acid Binding Factors Involved in Epidermal Differentiation

(A) Schematic setup of the screen; siRNA transfection (n = 20) is followed by induction of differentiation (n = 3, 5 conditions, 48 hr) and quantification of protein levels of transglutaminase 1.

(B–F) Volcano plots describing the effects of siRNA-based perturbation on transglutaminase 1 (TGM1) protein expression (x axis) and their significance (y axis) (n = 3) in vehicle (B), AG1478 (C), BMP2/7 (D), AG1478+BMP2/7 (E), and serum (F) treatment conditions. Data from chromatin factors (CFs) are displayed in red and nucleic acid (NA) binding factors in blue. Bars on top of graphs indicate spread of *Z* scores for each condition. FDR 0.001 (Benjamini-Hochberg). Differentiation induced for 48 hr using the indicated treatments (vehicle control, AG1478, BMP 2/7, AG1478 + BMP 2/7, serum).

(G) The top 5 most significant genes in each condition, of which knockdown results in down- or upregulation of transglutaminase 1 levels in the 5 different conditions. Significance is added as $-\log_{10}$(p value).

See also Figures S1 and S2.

may be important in the skin, as there are several genes that display isoform specific expression in different keratinocyte cell states. For instance, dermokine, a gene that is highly expressed in the granular layer of the epidermis, is heavily spliced, generating multiple isoforms with different functions (Naso et al., 2007). Another example is desmoplakin (DSP), which has two major isoforms that seem to have distinct functions in controlling desmosomal adhesion in the skin (Cabral et al., 2012). These examples illustrate the importance of proper regulation of both transcriptional and post-transcriptional processes. However, our current understanding of how these processes coordinately govern epidermal biology is limited.

Here, we investigated the role of 145 putative DNA and/or RNA binding factors in human epidermal differentiation using small interfering RNA (siRNA)-based perturbation screens. We identified the matrin type-2 zinc-finger protein ZMAT2 as being important to maintain cells in an undifferentiated state and as a splicing regulator of adhesion-related transcripts. Moreover, computational predictions and experimental validation uncovered a previously unappreciated connection between epigenetic and post-transcriptional control of keratinocyte differentiation.

RESULTS

Gene Perturbation Screens Identify Nucleic Acid-Binding Proteins Involved in Human Keratinocyte Renewal and Differentiation

To investigate the role of putative nucleic acid-binding factors in the regulation of epidermal stem cell renewal and differentiation, we performed siRNA-based knockdown screens (Figure 1A). For this, we selected 145 genes based on their expression levels in keratinocytes (reads per kilobase million [RPKM] >5), differential expression during differentiation (Figures S1A and S1B) (Kouwenhoven et al., 2015), and DNA or RNA binding potential. To test the contribution of these genes to the process of differentiation, we silenced each gene using a pool of 3 independent siRNAs in triplicate and subsequently induced differentiation. Transfected cells were cultured in different conditions for 48 hr to induce differentiation with the EGF inhibitor AG1478, BMP 2/7, a combination of these compounds, 10% fetal bovine serum, and a vehicle control, as previously described (Mulder et al., 2012). These treatments led to the robust induction of terminal differentiation marker TGM1 (Mulder et al., 2012). Endogenous TGM1 protein was quantified using a fluorescent In-Cell

Western assay with an antibody (BC.1), whose specificity was confirmed using 2 independent siRNAs (Figure S1C). To account for differences in cell number among the knockdown populations in the screen, TGM1 measurements were normalized on DNA content (DRAQ5 signal) for each well. After *Z* score transformation, the results were compiled into a single dataset covering all 145 genes, 5 conditions, and replicates (Data S1). High correlation between replicates highlighted the reproducibility of our findings and the quality of our dataset (Figure S1D). Using a random selection of 11 genes, we estimated the median knockdown efficiency to be 88% (range: 28%–93%) and the false-negative rate at <10% (Figure S1E). In addition, we performed deconvolution experiments in which the individual siRNAs were tested in parallel with the pool of 3 siRNAs that was used in the screen. This indicated that 71%–87% of the siRNA pools contained at least 2 siRNAs that recapitulated screen results (Figure S1F), which argues against widespread off-target effects. Our dataset constitutes a high-quality resource of nucleic acid binding factors to further characterize for their role in epidermal self-renewal and differentiation.

From these data we identified putative nucleic acid binding factors that significantly affected TGM1 levels (Benjamini-Hochberg [BH] false discovery rate [FDR] $p < 0.001$) compared to the average across all siRNAs in the screen in any of the conditions (Data S1; Figures 1B–1F, blue datapoints). The normalized effect size per gene is plotted on the x axis, whereas the statistical significance is depicted on the y axis. These representations of the data highlight the factors that modulate differentiation in the top left and top right quadrants, respectively. Notably, the effects and significance of individual factors were condition dependent, indicating that not all identified factors play equivalent roles in the different conditions tested (Data S1; Figure S2A). This is represented by the partial correlation between the effect sizes across the conditions (Figure S2A, scatterplots in bottom half) and the significant differences when comparing different conditions (Figure S2A, volcano plots in top half). In total, our screens revealed 57 genes that display a significant effect in at least 1 of the conditions (Data S1), indicating that our experiments identified factors that have a potential regulatory role in keratinocyte differentiation.

To explore these individual hits, we selected the top 5 most significant genes (Benjamini-Hochberg FDR $p < 0.001$) for each condition (Figure 1G). These represent 21 distinct nucleic acid binding factors, one-third of which (7) have previously been implicated in epidermal renewal and/or differentiation, confirming the validity of our approach (Nagarajan et al., 2010; Botti et al., 2011; Kolev et al., 2008; Tsuji et al., 2018; van den Bogaard et al., 2015; Mehic et al., 2005; Marthaler et al., 2017; Tribioli et al., 2002; Bourke et al., 2017; Amendt et al., 2002; Albino et al., 2012). We sought to experimentally verify that the TGM1 measurements in our screen represented bona fide differentiation and not solely regulation of TGM1 levels. To this end, we selected IRF6 and ETS1 as exemplars and used RT-qPCR as an alternative readout of the expression of differentiation and basal cell markers after siRNA-mediated silencing. IRF6 has been shown to be important for the expression of genes critical to epidermal differentiation (Botti et al., 2011). In addition, ETS1 is involved in keeping the cells in an undifferentiated state by repressing genes involved in the formation of the cornified envelope (Nagarajan et al., 2010). RT-qPCR analysis confirmed the effects of the knock down of these genes on TGM1 protein levels in our experiments (Figure S1G). Moreover, we found that silencing IRF6 resulted in lower expression of the differentiation markers PPL, ENV, and IVL, whereas ETS1 silencing resulted in induction of these differentiation markers and a reduction in the basal cell markers ITGA6 and ITGB1. This is in line with the literature in which IRF6 is thought to regulate differentiation and ETS1 is important in the self-renewing state. These results also confirm that the effects of silencing IRF6 or ETS1 in our screen reflect the cellular differentiation state and not merely deregulation of TGM1 expression.

ZMAT2 Maintains Epidermal Keratinocytes in an Undifferentiated, Proliferating State

A powerful feature of the approach we took is that our siRNA-based screen setup allows us to combine the current results on 145 DNA and/or RNA binding factors with published data characterizing ~330 epigenetic regulators (Mulder et al., 2012). Moreover, it enables us to use a previously developed Bayesian statistical framework that reveals genes that functionally interact (Wang et al., 2012). This means identifying sets of genes that share functionality through the regulation of similar cell biological processes—in this case epidermal differentiation. Applying this statistical approach to a combined epigenetic and DNA and/or RNA binding factor dataset should therefore allow identification of functional interactions among these groups of genes, leading to insights into their joint regulation of epidermal biology. The data distribution and variation of the two datasets are highly comparable, allowing us to combine them for further analysis (Figures 1B–1F, boxplots, and S2B). This resulted in a rich dataset comprising 473 genes describing their effects on the expression of TGM1 in 5 conditions. Application of the Bayesian network algorithm to this joint dataset revealed strong predicted functional interactions between ZMAT2, a matrin-type 2 like zinc-finger with potential DNA or RNA binding capacity, and components of a previously identified network of epigenetic regulators involved in epidermal renewal (Mulder et al., 2012) (Figures 2A and S3, full network). This subnetwork contained multiple members of different protein complexes representing diverse epigenetic mechanisms such as MORF complex members ING5 and BRD1, NURF complex members BPTF and SMARCA5, and SMARCC2 and UHRF1 (Mulder et al., 2012). This implies that ZMAT2 plays a role in epidermal differentiation in conjunction with these epigenetic modifiers.

These predicted functional interactions prompted us to functionally characterize ZMAT2 further. RT-qPCR analysis showed that silencing ZMAT2 in keratinocytes resulted in increased expression of differentiation markers (PPL, EVPL, INV, TGM1) and concordant downregulation of basal-cell markers ITGB1 and ITGA6 (Figure 2B). In addition, depletion of ZMAT2 resulted in a strong reduction in the number and size of clones in the colony formation assay (Figure 2C), reflecting a loss of cell renewal and proliferation capacity. These effects were not associated with increased cell death or the induction of apoptosis following ZMAT2 depletion (Figures S4A and S4B). Furthermore, cell-cycle analysis showed that there was no immediate defect in

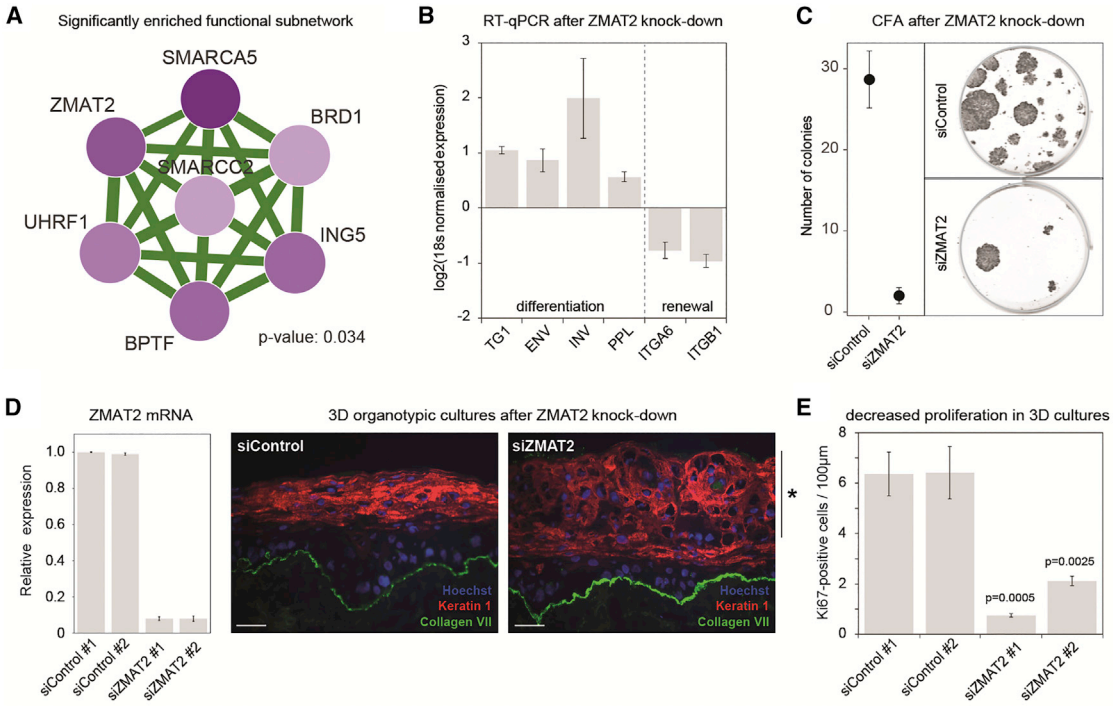

Figure 2. Bayesian Network Prediction Reveals a Functional Interaction Network between Epigenetic Factors and ZMAT2

(A) The significant subnetwork predicting functional interactions between epigenetic factors ING5, SMARCA5, SMARCC2, BRD1, BPTF, and UHRF1 and zinc-finger ZMAT2. (n = 3, an empirical p value was determined using a bootstrapping approach).

(B) RT-qPCR based characterization (n = 3, average log2 over non-targeting control siRNA [siControl] ± SD) of siZMAT2 depleted keratinocytes (no additional induction of differentiation was applied).

(C) Colony formation assays (n = 3, average ± SD) of ZMAT2-depleted cells.

(D) Left: RT-qPCR analysis of knockdown efficiency in 3D cultures. Right: immunofluorescent staining of 3D organotypic cultures cultured after transfection with siZMAT2 (n = 3, average ± SD; blue represents Hoechst 33342, red represents KRT1, and green represents ColVII). Scale bar represents 50 μm. Asterisk indicates morphologically disorganized epidermis.

(E) Quantification of Ki67$^+$ basal cells per 100 μm (n = 3, average ± SD) in the transfected 3D organotypic cultures. p value calculated with 2-sided t test.

See also Figures S3 and S4.

proliferation (72 hr post-siRNA transfection), indicating that the decrease in colony number and size in the colony formation assay (CFA) is caused by an effect on long-term proliferation (Figure S4C). This is also recapitulated in 3D organotypic cultures (Figure 2D), showing that knock down of ZMAT2 causes a marked decrease in the number of proliferative cells (Ki67$^+$ cells quantified by immunostaining) and a disorganized epidermis compared to non-targeting control siRNA (siControl) (Figure 2E, 2–4 independent cultures with 2 independent siRNAs). These results indicated that ZMAT2 plays a role in maintaining epidermal cells in an undifferentiated, proliferative state and confirms our primary screen results.

ZMAT2 Functionally Interacts with Epigenetic Regulators of Epidermal Cell Renewal

The Bayesian mixture model predicted that ZMAT2 functionally interacts with the epigenetic regulators ING5, SMARCA5, BPTF, UHRF1, and BRD1. We aimed to confirm these predicted interactions using a double knockdown strategy. In this way, true functional interactions can be identified (Mani et al., 2008; Costanzo et al., 2010; Horn et al., 2011; Roguev et al., 2013) by comparing the quantitative effects of combinatorial knockdowns on global gene expression with effects that can be expected based on the individual knockdown (Horn et al., 2011). In cases in which 2 genes are functionally independent (i.e., do not functionally interact), the observed phenotype in the double knockdown is equivalent to the product of the individual knockdown phenotypes, or, when working with log-transformed values, their summed value (Mani et al., 2008; Costanzo et al., 2010; Horn et al., 2011; Roguev et al., 2013). Using this "product rule" as the null hypothesis (labeled "exp" for expected in Figure 3A), genetic interactions are statistically defined as aggravating (when the observed phenotype is greater than expected) or alleviating (when the observed phenotype of the combined knockdown is less pronounced than expected), respectively (Figure 3A). In general, alleviating interactions occur between genes involved in the same process and/or pathway, whereas aggravating interactions tend to be associated with functionally redundant processes (Costanzo et al., 2010; Roguev et al., 2013).

In previous work, we showed that the epigenetic regulators within the predicted subnetwork (Figure 2A) display true functional interactions (Mulder et al., 2012). Therefore, we decided

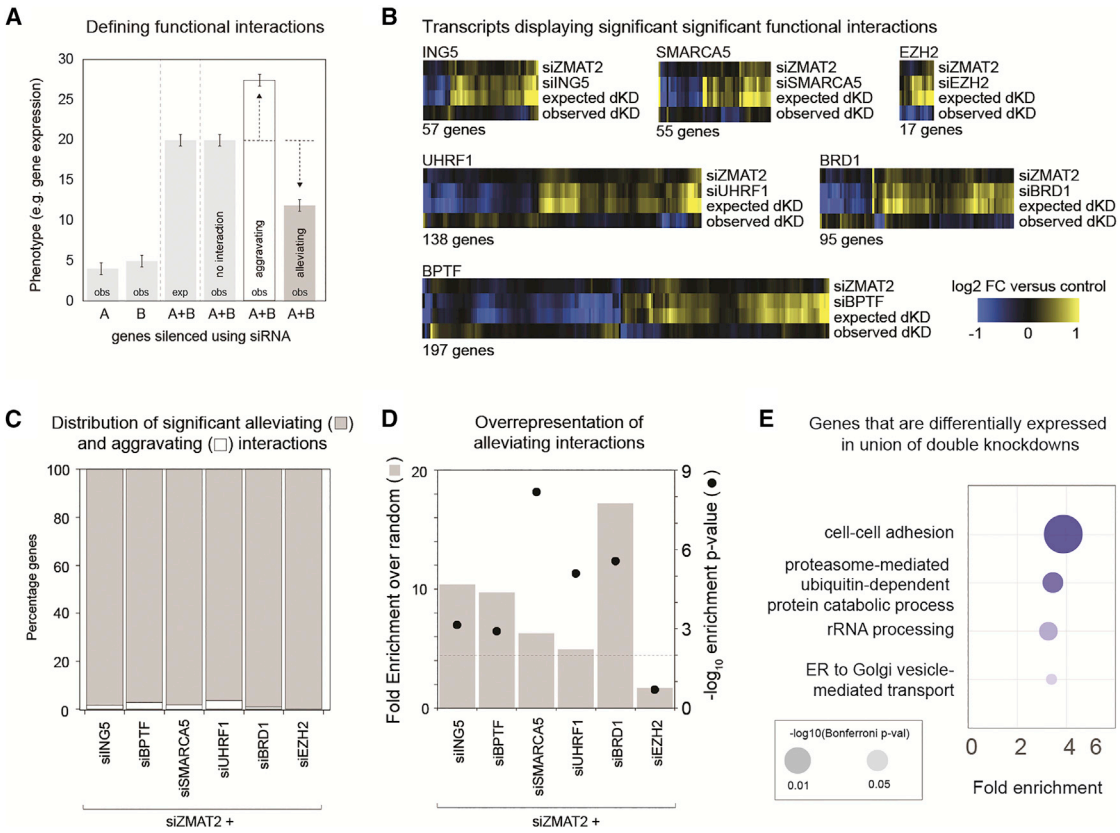

Figure 3. ZMAT2 and the Epigenetic Factors Regulate Similar Processes in Epidermal Differentiation

(A) Schematic depiction of the definition of aggravating and alleviating functional interactions. obs, observed. exp, expected (statistical null model).

(B) Heatmaps visualizing differential expression within the different samples. Scale represents log2 fold-change over siControl. Multiple testing corrected $p < 0.01$, two-sided t test.

(C) Distribution of the statistically significant aggravating and alleviating functional interactions for each of the combined knockdown experiments.

(D) Enrichment of alleviating interactions in functionally interacting transcripts compared to random. p value calculated using a hypergeometric test.

(E) Gene Ontology term analysis on the union of all significantly differentially expressed genes within the knockdown combinations (DAVID). Multiple testing corrected p value calculated using a hypergeometric test. ER, endoplasmic reticulum.

to experimentally test the predicted interactions between ZMAT2 and ING5, SMARCA5, BPTF, UHRF1, or BRD1 using a combined knockdown approach. As a control, we included EZH2, which is only peripherally associated with the epigenetic factors in this network (Mulder et al., 2012). To obtain a detailed quantitative phenotype representing the cell state, we performed RNA-sequencing expression profiling after silencing each of these epigenetic factors individually, as well as in combination with ZMAT2. Two independent siRNAs targeting each gene were used in all of the possible permutations in triplicate. We analyzed a total of 156 knockdown samples using a modified CEL-seq2 method that enables high-throughput 3′ end tag-counting RNA-sequencing (see STAR Methods for details). It is important to note that the relatively shallow RNA-sequencing we performed does not allow us to directly interpret the molecular mechanisms underlying these interactions, but it is powerful for the discovery of functional interactions based on the obtained RNA expression profiles. We examined the data using DESeq 2.0 and identified transcripts that were significantly differentially expressed ($p < 0.05$) compared to control siRNA-transfected cells. After quality control and filtering (see STAR Methods), we labeled an interaction alleviating or aggravating for each detected transcript per interrogated combination. We identified the transcripts that displayed a statistically significant genetic interaction based on the product rule criteria, as explained above (Figure 3A, Benjamini-Hochberg FDR $p<0.01$). For each of the factors we silenced in combination with ZMAT2, between 55 and 197 genes displayed such interactions, in which the peripherally associated factor EZH2 showed only 17 functionally interacting transcripts (Figure 3B). The vast majority (>95%, in all cases) of the identified functional interactions were alleviating interactions (Figure 3C). Moreover, these alleviating interactions were highly enriched compared to randomly picked genes (Figure 3D). This suggests that ZMAT2, ING5, SMARCA5, BPTF, UHRF1, and BRD1 function in a similar process and/or pathway to affect epidermal biology. Next, we performed Gene Ontology (GO) term enrichment analysis on the genes contributing to the observed functional interactions and found an overrepresentation of factors involved in cell adhesion, a process that is required for anchoring epidermal stem cells to their niche (Figure 3E). These findings

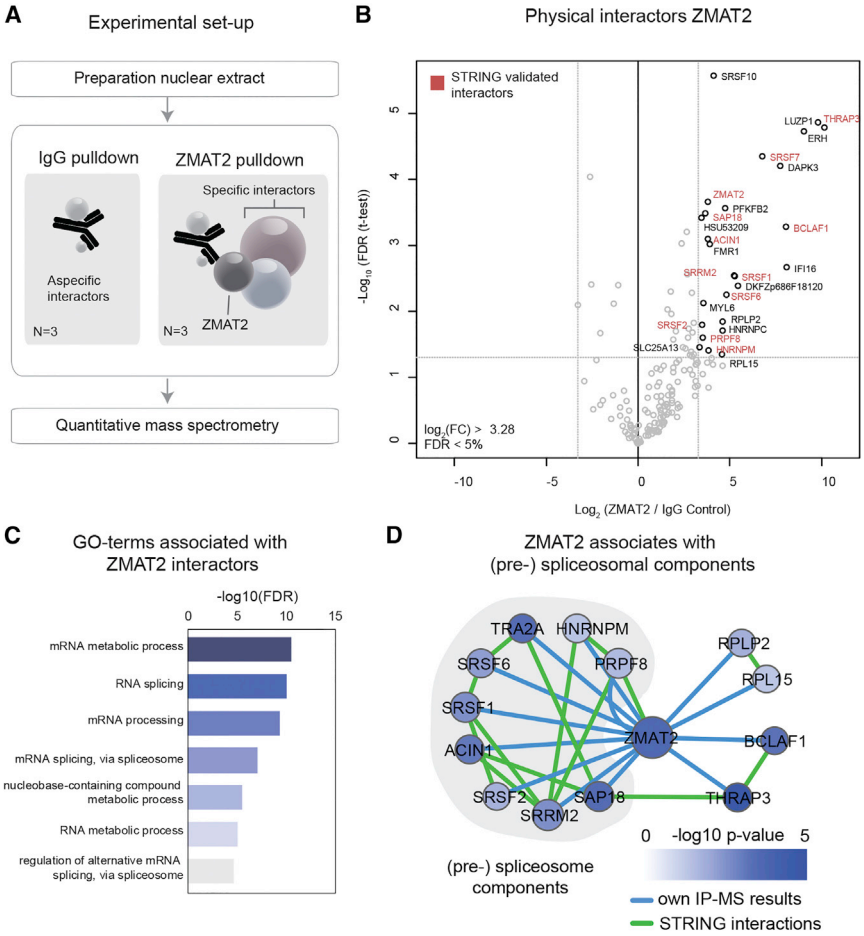

Figure 4. ZMAT2 Interacts with Components from the Pre-spliceosome

(A) Schematic representation of the experimental setup. Nuclear extract was prepared, one in which IgG and ZMAT2 pull-downs were performed in triplicate. The peptides were quantified using label-free mass spectrometry.

(B) Volcano plot displaying the physical interactors of ZMAT2, with the log2 fold enrichment of ZMAT2 associated proteins over non-specific IgG-bound proteins plotted against their significance (n = 3). Multiple testing corrected p value calculated with a 2-sided t test.

(C) Gene Ontology term analysis (STRING) on proteins associated with ZMAT2. Multiple testing corrected p value calculated using a hypergeometric test.

(D) STRING interactions versus experimentally found interactions with their significance (as calculated in B) displayed in blue.

See also Figure S5.

show that we were able to experimentally validate the predicted functional interactions between these epigenetic factors and ZMAT2 and that this group of genes jointly regulates an RNA expression program linked to cell adhesion.

ZMAT2 Associates with the (Pre-)spliceosome in Epidermal Keratinocytes

To gain insight into the potential molecular role of ZMAT2 in epidermal cell biology, we identified the proteins it associates with using immunoprecipitation and quantitative mass spectrometry (IP-MS; Figure 4A). Reminiscent of the epigenetic factors, the ZMAT2 protein localizes to the nucleus, as determined by immunofluorescence microscopy (Figure S5A). Antibody specificity was confirmed using siRNA-mediated knockdown, resulting in decreased nuclear ZMAT2 staining (Figure S5A). Next, we performed immunoprecipitation (IP) using control immunoglobulin G (IgG) (non-targeting and background binding) and antibodies targeting endogenous ZMAT2 from nuclear extracts in triplicate. Following IP, sample preparation, and desalting, these samples were subjected to label-free quantitative mass spectrometry to identify associated proteins. The data are represented as enrichment over IgG control versus the significance over the 3 replicates, with significant interactors located in the right upper quadrant (Figure 4B). Both Gene Ontology and protein interaction database analysis of the interacting proteins revealed that ZMAT2 interacts with components of the (pre-)spliceosome (Figures 4C and 4D). These findings are in line with recent cryoelectron microscopy (cryo-EM) structures of the budding yeast pre-spliceosome, showing that the putative ZMAT2 ortholog Snu23 associates with the B* (pre-catalytic) complex (Plaschka et al., 2017; Ulrich and Wahl, 2017). Our biochemical experiments identifying ZMAT2 as an interactor of the pre-spliceosome in human keratinocytes, together with our screen and validation analysis, implicate RNA splicing as a potential key regulatory process in epidermal renewal and differentiation.

ZMAT2 Associates with a Subset of Cellular Transcripts Involved in Epidermal Biology

Even though mRNA splicing is a ubiquitous process, we wondered whether ZMAT2-containing spliceosomes display selectivity toward specific transcripts or whether ZMAT2 is associated with essentially all of the transcripts present in the cell. An indication for a more selective role for ZMAT2 stems from the observation that the ZMAT2 protein is expressed in a tissue-specific manner, whereas other pre-spliceosome components show much more ubiquitous expression in the human body (Figure S5B). Another indication comes from the Gene Ontology term analysis on the genes that are regulated by the functionally connected genes in our double knockdown experiments, where we found an enrichment of adhesion-related genes (Figure 3E). To identify ZMAT2-associated transcripts, we performed RNA IP-sequencing (RIP-seq) with non-specific control IgGs and ZMAT2-specific antibodies from nuclear extracts. RNA-IPs were performed in triplicate, and the isolated RNA was used to generate RNA-sequencing libraries using the modified CEL-seq2 protocol (Figure 5A). This specific form of library

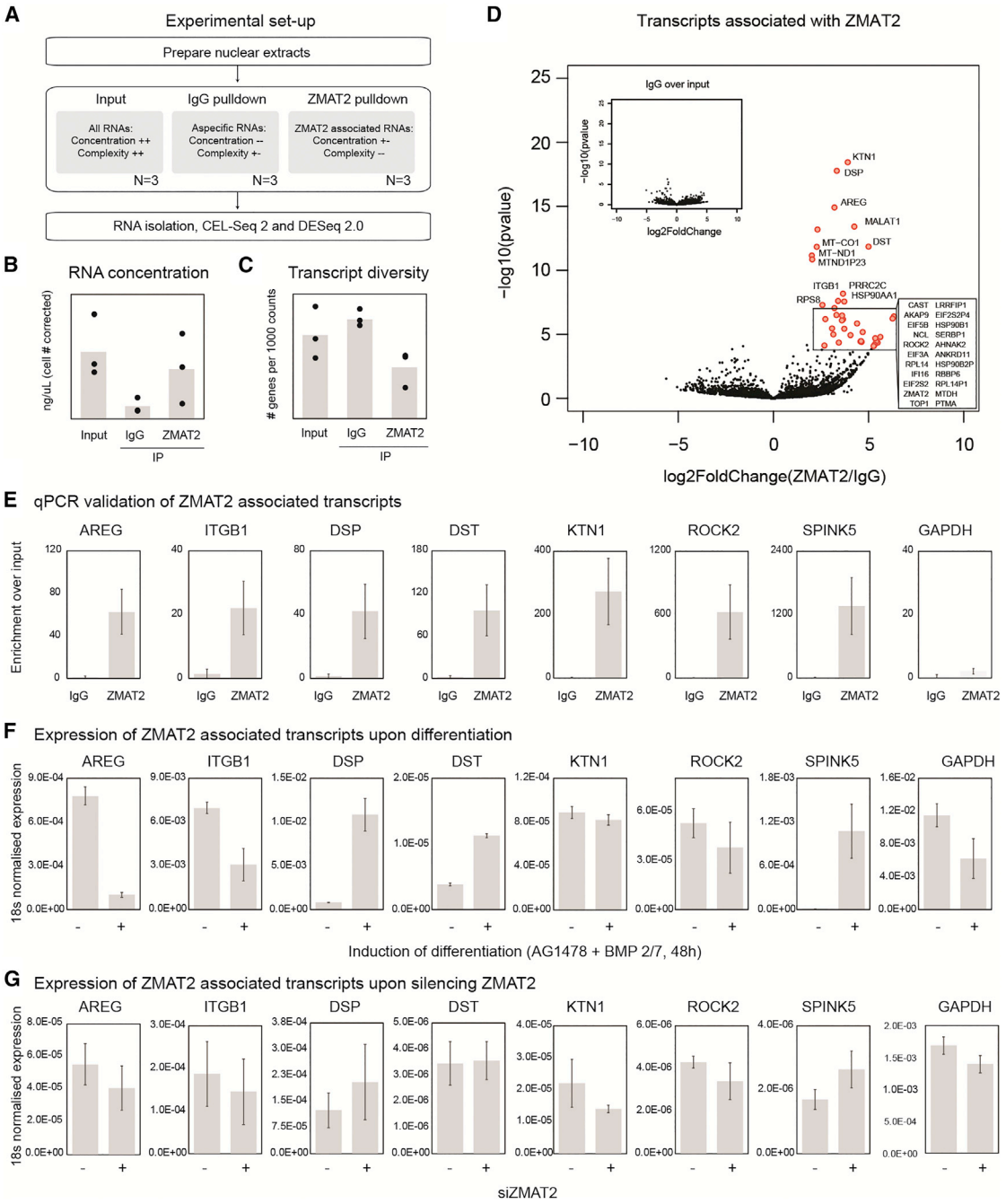

Figure 5. Adhesion-Related Transcripts Are Associated with ZMAT2

(A) Schematic representation of the experimental setup. Nuclear extract was prepared from non-differentiated cells, and the normal immunoprecipitation procedure was performed up to the wash steps. RNA was isolated directly from the beads and prepared for sequencing using CEL-seq2.

(B) RNA concentration samples before and after the immunoprecipitation (IP) procedure. Corrected for cell numbers, in nanograms per microliter (n = 3).

(C) Transcript diversity of the CEL-seq2 libraries after sequencing. Number of identified genes per 1,000 counts (n = 3).

(D) Volcano plot displaying the transcripts that are significantly enriched in the ZMAT2 IP sample over the IgG IP sample as called by DESeq 2.0. Inset represents significant hits identified in the IgG sample (n = 3). Multiple testing corrected p value calculated with a 2-sided t test.

(E) qPCR validation of ZMAT2-associated transcripts in the IP samples showing the enrichment over the input sample (n = 3, average ± SEM).

(F) Expression of the ZMAT2-associated transcripts is differential during induction of differentiation using EGF inhibitor AG1478 (10 μM) and BMP 2/7 for 48 hr (n = 3, average ± SEM).

(G) Expression of ZMAT2-associated transcripts upon silencing ZMAT2 (70% knockdown [KD], 5 days of culture), as determined via qPCR (n = 3, average ± SD).

preparation focuses on polyadenylated transcripts and allows analysis of the low amount of material retrieved after IP. To assess the specificity of enrichment, the recovered transcripts were compared to RNA-sequencing of the input material. Although the same amount of input material for IgG and ZMAT2 pull-downs was used, the IP with the ZMAT2 antibodies yielded substantially more RNA compared to the control IgGs, as can be expected from its association with the spliceosome (Figure 5B). The library transcript diversity (number of different transcripts detected per 1,000 reads) of the RNAs associated with the control IgGs was similar to that of the input, reflecting non-specific interactions. In contrast, the diversity of the ZMAT2-associated RNAs was lower, indicating that ZMAT2 associates with a subset of the total available transcripts, rather than binding RNAs indiscriminately (Figure 5C).

Next, we used statistical analysis (DESeq 2.0) to identify significantly enriched transcripts for both the IgG and the ZMAT2 samples. None of the RNAs identified in the control IgG IP were significantly enriched compared to inputs, indicating that these represented non-specific background interactions (Figure 5D, inset). In contrast, nearly 100 transcripts were significantly enriched in the ZMAT2 pull-down (Figure 5D). We chose to use the IgG data as a comparison for the ZMAT2 sample to ensure that we were comparing samples that had been processed in an identical fashion. Many of the transcripts that were specifically and strongly associated with ZMAT2 are involved in cell adhesion (e.g., ITGB1 [Levy et al., 2000], DSP [Cabral et al., 2012], DST [Michael et al., 2014], and ROCK2 [Lock et al., 2012]) and proliferation processes (e.g., AREG [Stoll et al., 2016]). Because both the functional interaction and RNA-IP experiments point toward regulation of adhesion, we decided to focus on these transcripts. We selected 7 of these transcripts for validation by RNA-IP, followed by RT-qPCR, and included glyceraldehyde 3-phosphate dehydrogenase (GAPDH) as a negative control. This confirmed that all 7 transcripts are highly enriched in the ZMAT2 pull-downs, whereas GAPDH is not, confirming the selectivity of RNAs associated with ZMAT2 (Figure 5E). The lack of enrichment of GAPDH, one of the most abundantly expressed transcripts, in the ZMAT2 pull-down indicated that the identified associations are not solely based on transcript abundance. Moreover, of these 7 transcripts, ITGB1, AREG, DSP, DST, and SPINK5 are differentially expressed during differentiation (Figure 5F), suggesting that at least some of the ZMAT2-associated transcripts are also regulated at the transcriptional level. However, ZMAT2 itself does not seem to be involved in the regulation of their expression, because silencing ZMAT2 does not affect the expression of ITGB1, ROCK2, AREG, and DST. The mild differential expression of KTN1 (downregulated) and DSP and SPINK5 (upregulated) are likely an effect of ZMAT2 silencing on the differentiation state of the cell (Figures 2B and 5G). These experiments indicate that ZMAT2 associates, presumably through its interaction with the pre-spliceosome, with a specific subset of transcripts in human epidermal cells.

ZMAT2 Silencing Leads to Differential Exon Usage of Selected Genes

To investigate whether ZMAT2 silencing affects splicing in our cells, we performed full-length transcript RNA-sequencing on ZMAT2 knockdown samples in triplicate (Figure 6A). We included the ZMAT2 interacting pre-spliceosome component SRSF1 as a positive control for the disruption of splicing (Figure 4B). Silencing SRSF1 is expected to lead to defects in splicing because it is involved in the first steps of assembly of the spliceosome by enhancing the binding of the U1 small nuclear ribonucleoprotein particle (snRNP) on the pre-mRNA (Kohtz et al., 1994). In addition, we analyzed samples in which we induced differentiation (48 hr, AG1478 + BMP2/7), to put our findings in the context of keratinocyte differentiation. DEXSeq (Anders et al., 2012) was used to calculate and statistically assess differential exonic region usage for all identified transcripts to detect altered splicing activity. This revealed that ZMAT2 affects splicing, although fewer exonic regions are affected in their splicing by silencing ZMAT2 compared to silencing SRSF1 or induction of differentiation—~0.12 versus ~1.5% for SRSF1 and 4% after induction of differentiation, respectively (Figure 6B). These are consistent with the notion that that ZMAT2 regulates splicing of a more restricted set of transcripts than SRSF1 and the set that is differentially spliced in differentiation. Moreover, the majority of exonic regions that are differentially spliced upon silencing of ZMAT2 are also differentially spliced in differentiation (Figure 6C), indicating that ZMAT2 is involved in mediating splicing events associated with differentiation and that regulating splicing of specific subset of genes plays a role in epidermal biology. In line with this, organotypic cultures of cells depleted of SRSF1 displayed an expanded and disorganized epidermal layer, while also affecting proliferation as determined using Ki67 staining (Figures S6A–S6C). Thus, silencing the spliceosome component SRSF1 (at least partially) phenocopies ZMAT2-depleted epidermis (Figures 2C and 2D), confirming the role of splicing regulation in epidermal biology.

Exon usage of nearly 200 transcripts was affected by both ZMAT2 and SRSF1. Of these 200 transcripts, the exons that were differentially regulated by these factors were predominantly mutually exclusive (Figure 6D), further supporting the notion of specific functions for ZMAT2 compared to the core pre-spliceosome component SRSF1 in epidermal keratinocytes. An exemplar of this is the DMKN gene, which we experimentally validated using exon-specific RT-qPCR (Figures S6E and S6F). DMKN plays an important role in epidermal cornification and is extensively spliced during differentiation (Naso et al., 2007; Leclerc et al., 2014). We observed altered usage of exonic regions in the N-terminal part of the transcript in the absence of ZMAT2, which is also differentially spliced upon the induction of differentiation (Figures S6E and S6F). Notably, we also observed specific ZMAT2- and SRSF1-dependent differentially spliced exonic regions. This further confirms that the observed differential splicing in the small interfering RNA targeting ZMAT2 (siZMAT2) samples are likely ZMAT2 dependent, rather than general differentiation-mediated splicing following ZMAT2 silencing.

To investigate whether there were differences in the usage of specific splicing mechanisms between ZMAT2 and SRSF1, we used the MISO package, which enables a differential splicing analysis based on annotation files describing different splice events. This did not reveal major differences in splicing mechanisms (skipped exons [SEs], intron retention [RI], mutually exclusive exons [MXEs], alternative 5′splice sites [A5SSs], or

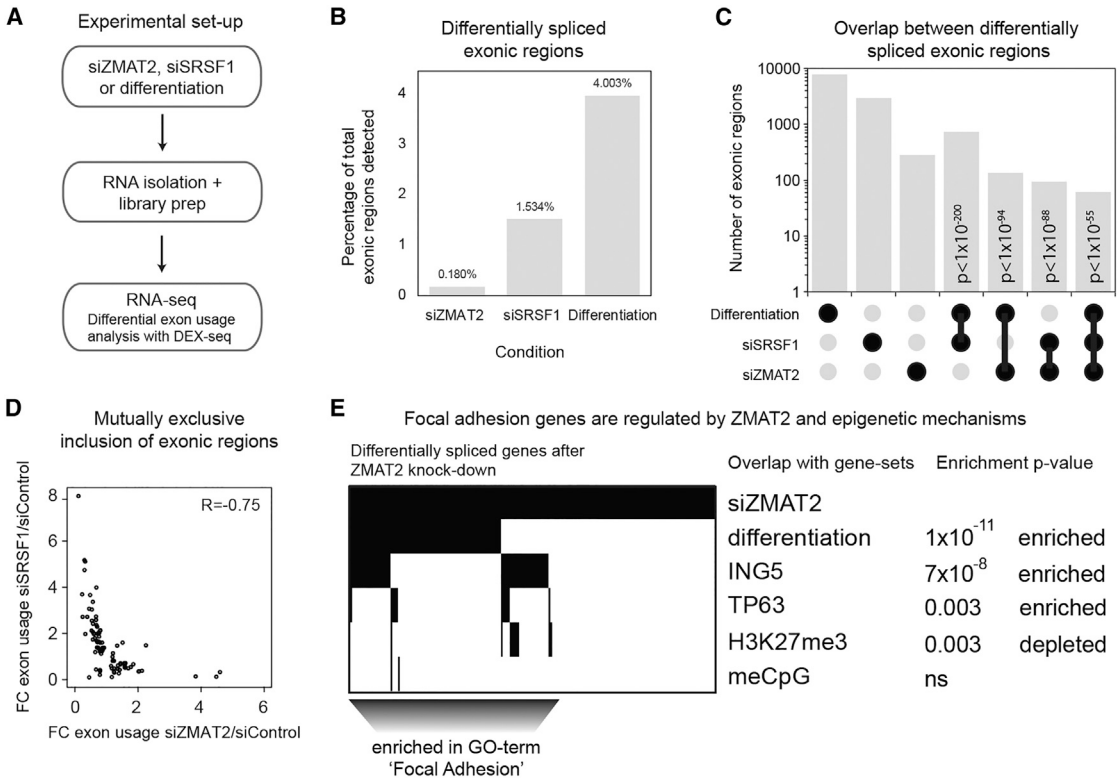

Figure 6. ZMAT2 Regulates a Similar Gene Set as the Functionally Interacting Epigenetic Factors through Modulation of RNA Splicing

(A) Schematic representation of the experimental setup. ZMAT2 or SRSF1 was silenced using siRNAs, and cells were grown for 5 days or differentiation was induced (48 hr, AG1478 + BMP 2/7), after which RNA was isolated and sequencing libraries prepared. Analysis was performed using DEXSeq.

(B) Percentage of total detected differentially spliced exonic regions as determined with the DEXSeq package in samples transfected with siZMAT2 or siSRSF1 or where differentiation was induced.

(C) Overlap differentially spliced exonic regions for samples transfected with siZMAT2 or siSRSF1 or where differentiation was induced. p values were calculated with a hypergeometric test.

(D) Differential usage exonic regions, plotting the fold change over siControl versus siSRSF1 or siZMAT2 (average of n = 3). *R*, Pearson's correlation.

(E) Differentially spliced genes after knockdown of ZMAT2 are enriched for the binding of ING5 (chromatin immunoprecipitation sequencing [ChIP-seq] data [Mulder et al., 2012]) and keratinocyte master regulator TP63. Gene Ontology term analysis on these genes shows enrichment for focal adhesion-related terms. p values were calculated with a hypergeometric test.

See also Figure S6.

alternative 3′ splice sites [A3SSs]) affected by ZMAT2 compared to SRSF1 (Figure S6D). Moreover, computational analysis did not identify strong motifs specifically associated with ZMAT2-dependent splicing events compared to SRSF1-mediated splicing. Together, our experiments suggest that ZMAT2 regulates exon usage of a specific subset of transcripts rather than functioning as a global splicing regulator in epidermal stem cells. We note that our splicing analysis is unlikely to be fully comprehensive, because there is a slight enrichment of high expressed transcripts in our data, precluding the interrogation of low expressed genes.

Functionally Interacting Genes Jointly Regulate an Expression Program Involved in Cell Adhesion

The above-presented results, together with the network prediction and functional interaction experiments (Figures 2 and 3), indicate that there is a link between epigenetic regulation and ZMAT2-mediated splicing of genes involved in cell adhesion. Consistent with these functional interactions, we found that the transcripts that are affected in their exon usage upon ZMAT2 silencing are highly enriched ($p < 10^{-8}$) in direct ING5 genomic binding targets, one of the epigenetic factors in the functional interaction network (Figure 6E) (Mulder et al., 2012), indicating that these genes regulate similar processes. In contrast, there was no clear evidence for overlap with genes marked by DNA methylation or the heterochromatin-associated H3K27me3 histone modification. Moreover, only a slight enrichment ($p = 0.003$) for targets of the key epidermal transcription factor TP63 was found, suggesting that ING5 and ZMAT2 cooperate to regulate an RNA expression program that is important for epidermal biology. Notably, the gene program targeted by both ZMAT2 and ING5 was further enriched in genes associated with focal adhesion formation, a process that anchors epidermal stem cells to their niche. Overall, we conclude that joint epigenetic and splicing regulation of specific subsets of genes maintains epidermal stem cells in a proliferative, undifferentiated state.

DISCUSSION

Our results indicate that regulation of cell-cell adhesion-related transcripts is at least orchestrated by a set of chromatin-associated epigenetic regulators and a splicing component. We were able to discover their joint contribution by considering how genes cooperate in the regulation of gene expression programs, starting from our siRNA-based screens. Through these experiments we generated a rich dataset describing the roles of DNA and/or RNA binding factors and epigenetic regulators in human epidermal stem cell differentiation. The specific setup of the experiments enabled us to use our previously published network Bayesian algorithm that predicts functional relations between genes, transcending the annotation of a gene as a transcription factor, chromatin modifier, or splicing factor and providing insight into how genes and processes work together to shape epidermal biology. Using this approach, we uncovered functional interactions between chromatin factors representing different epigenetic mechanisms and the uncharacterized zinc-finger-containing protein ZMAT2. Through interaction proteomics and RNA-sequencing approaches we found that ZMAT2 is involved in RNA splicing in epidermal keratinocytes. Moreover, RNA interaction experiments revealed an enrichment of adhesion-related genes, suggesting that there is a targeted process involved. Thus far, we did not find evidence for specific deregulated splicing mechanisms that could explain this selectivity, nor could it be explained simply through transcript abundance and/or occurrence of specific RNA motifs.

It is conceivable that ZMAT2 functions through fine-tuning the splicing mechanism of a subset of genes, especially when considering the different steps involved in splicing and the potential role for ZMAT2 in these. Splicing is an important post-transcriptional mechanism that catalyzes the excision of non-coding parts in pre-mRNA transcripts or, in alternative splicing, the exon composition in a mature mRNA transcript. It is regulated by the large and dynamic spliceosome complex, which facilitates the different steps of the splicing reaction through rearrangements in protein composition for each step. In the first step, the so-called complex A recognizes the splice site, after which complex B is assembled. This complex is catalytically activated to the B* complex via the intermediate B^{act} complex. The B* complex catalyzes the first transesterification reaction and, after more rearrangements, generates complex C, which catalyzes the second transesterification reaction. The spliceosome is then disassembled and the subunits are recycled. ZMAT2 is an interactor of the B complex, where it accompanies the core complex B component tri-snRNP U4/U6.U5. In yeast, this tri-snRNP is already associated with ZMAT2 homolog Snu23 and pre-mRNA processing factor 38 (Prp38) strictly before integration into the yeast pre-spliceosome (Plaschka et al., 2017). In contrast, in humans these 2 proteins are recruited independently from the tri-snRNP and are therefore considered non-snRNP proteins. There are 7 more of these non-snRNP proteins in humans (Ulrich and Wahl, 2017), which are referred to as B-specific proteins. Although some of these proteins can influence splice-site selection (e.g., Smu1, RED) (Spartz et al., 2004), their exact function is not known. It is interesting to consider these proteins as mediators of alternative splicing through the recognition of different splice sites, which may explain the observed enrichment for adhesion-related genes for ZMAT2. However, even though the interaction of ZMAT2 with the human spliceosome seems less stringently required than it is in yeast, it may have an important function in enabling more general conformational changes from the B to the C complex. In yeast, Snu23 is thought to influence activation of the Brr2 helicase via its stabilization on the U4 snRNA, which is part of the U4/U6.U5 tri-snRNP. The Brr2-mediated unwinding of the U4/U6 duplex is an important step toward generating a catalytically active spliceosome because it frees the U6 snRNA to form an internal loop with the U2 snRNA. This enables the conformational changes needed for the branching step and subsequent exon ligation (Plaschka et al., 2017). It is possible that ZMAT2 transiently interacts with the human spliceosome to facilitate and fine-tune these transitions. If this is the case, then the timing of its association with the spliceosome may influence the efficiencies of competing splicing mechanisms, spliceosome composition, or conformation (Ulrich and Wahl, 2017). Although we can only speculate about the exact molecular mechanisms behind our observations at this point, the combined evidence from our proteomic data and the literature implicates ZMAT2 as a regulator of RNA splicing in epidermal stem cells.

Our results suggest that cell-cell adhesion is regulated by a previously unanticipated connection between transcriptional processes and post-transcriptional regulation. Experiments investigating the functional interactions between epigenetic modifiers and ZMAT2 revealed mostly alleviating interactions, stressing the importance of proper splicing in conjunction with epigenetic control of adhesion-related transcripts. We confirmed these connections experimentally by showing that the genes whose transcripts were differentially spliced upon silencing of ZMAT2 were enriched for the binding of ING5. Moreover, these genes were also enriched for the binding of p63, indicating that the functionally connected genes are in charge of regulating a gene set that is essential for epidermal biology. Considering the importance of proper regulation of adhesion signaling for maintaining the stem cell fate (Levy et al., 2000), it is not surprising that incorrect regulation leads to the severe effects observed upon silencing these genes individually. This in combination with the profound effect of silencing ZMAT2 individually on the differentiation state of the cells shows that the fine-tuning of splicing by ZMAT2 is of the utmost importance for keratinocyte biology.

We have discovered that this group of epigenetic modifiers and ZMAT2 represent important hubs in the regulation of adhesion-related transcripts and may be interesting to study more mechanistically in light of epidermal differentiation. We conclude that epigenetic and splicing factors jointly regulate processes that are essential for epidermal biology. Our work provides insights into the regulation of epidermal differentiation and highlights the importance of cooperation among disparate cellular processes in the regulation of cell behavior.

STAR★METHODS

Detailed methods are provided in the online version of this paper and include the following:

- KEY RESOURCES TABLE
- CONTACT FOR REAGENTS AND RESOURCE SHARING
- EXPERIMENTAL MODEL AND SUBJECT DETAILS

SUPPLEMENTAL INFORMATION

Supplemental Information includes six figures, one table, and one data file and can be found with this article online at https://doi.org/10.1016/j.celrep.2018.10.017.

ACKNOWLEDGMENTS

The authors would like to thank Dr. W. Mechelenbrink for advice on and help with the computational analyses, Bianca Förstl and Andrea Eder for their excellent technical assistance, and members of the Mulder lab for fruitful discussion. This work was supported by a VIDI grant from the Netherlands Organisation for Scientific Research (NWO-VIDI grant no. 864.12.010) to K.W.M.

AUTHOR CONTRIBUTIONS

S.E.J.T. designed, performed, and analyzed all of the experiments. P.W.T.C.J. and M.V. performed the proteomics experiments. S.J.v.H. performed the motif analysis on the RNA-sequencing data. H.Z. provided data prior to publication and interpreted data. M.K. performed and analyzed the 3D organotypic cultures. K.W.M. analyzed and interpreted the data and conceived and oversaw the study. S.E.J.T. and K.W.M. wrote the manuscript with input from all authors.

DECLARATION OF INTERESTS

The authors declare no competing interests.

Received: May 17, 2018
Revised: September 4, 2018
Accepted: October 3, 2018
Published: October 30, 2018

REFERENCES

Albino, D., Longoni, N., Curti, L., Mello-Grand, M., Pinton, S., Civenni, G., Thalmann, G., D'Ambrosio, G., Sarti, M., Sessa, F., et al. (2012). ESE3/EHF controls epithelial cell differentiation and its loss leads to prostate tumors with mesenchymal and stem-like features. Cancer Res. *72*, 2889–2900.

Amendt, C., Mann, A., Schirmacher, P., and Blessing, M. (2002). Resistance of keratinocytes to TGFbeta-mediated growth restriction and apoptosis induction accelerates re-epithelialization in skin wounds. J. Cell Sci. *115*, 2189–2198.

Anders, S., Reyes, A., and Huber, W. (2012). Detecting differential usage of exons from RNA-seq data. Genome Res. *22*, 2008–2017.

Biggs, L.C., Rhea, L., Schutte, B.C., and Dunnwald, M. (2012). Interferon regulatory factor 6 is necessary, but not sufficient, for keratinocyte differentiation. J. Invest. Dermatol. *132*, 50–58.

Botti, E., Spallone, G., Moretti, F., Marinari, B., Pinetti, V., Galanti, S., De Meo, P.D., De Nicola, F., Ganci, F., Castrignanò, T., et al. (2011). Developmental factor IRF6 exhibits tumor suppressor activity in squamous cell carcinomas. Proc. Natl. Acad. Sci. USA *108*, 13710–13715.

Bourke, L.M., Del Monte-Nieto, G., Outhwaite, J.E., Bharti, V., Pollock, P.M., Simmons, D.G., Adam, A., Hur, S.S., Maghzal, G.J., Whitelaw, E., et al. (2017). Loss of Rearranged L-Myc Fusion (RLF) results in defects in heart development in the mouse. Differentiation *94*, 8–20.

Cabral, R.M., Tattersall, D., Patel, V., McPhail, G.D., Hatzimasoura, E., Abrams, D.J., South, A.P., and Kelsell, D.P. (2012). The DSPII splice variant is crucial for desmosome-mediated adhesion in HaCaT keratinocytes. J. Cell Sci. *125*, 2853–2861.

Castro, M.A., Wang, X., Fletcher, M.N., Meyer, K.B., and Markowetz, F. (2012). RedeR: R/Bioconductor package for representing modular structures, nested networks and multiple levels of hierarchical associations. Genome Biol. *13*, R29.

Costanzo, M., Baryshnikova, A., Bellay, J., Kim, Y., Spear, E.D., Sevier, C.S., Ding, H., Koh, J.L., Toufighi, K., Mostafavi, S., et al. (2010). The genetic landscape of a cell. Science *327*, 425–431.

Cox, J., and Mann, M. (2008). MaxQuant enables high peptide identification rates, individualized p.p.b.-range mass accuracies and proteome-wide protein quantification. Nat. Biotechnol. *26*, 1367–1372.

Dobin, A., Davis, C.A., Schlesinger, F., Drenkow, J., Zaleski, C., Jha, S., Batut, P., Chaisson, M., and Gingeras, T.R. (2013). STAR: ultrafast universal RNA-seq aligner. Bioinformatics *29*, 15–21.

Eckert, R.L., Crish, J.F., Banks, E.B., and Welter, J.F. (1997). The epidermis: genes on – genes off. J.Invest. Dermatol. *109*, 501–509.

Eckert, R.L., Sturniolo, M.T., Broome, A.M., Ruse, M., and Rorke, E.A. (2005). Transglutaminase function in epidermis. J. Invest. Dermatol. *124*, 481–492.

Hashimshony, T., Senderovich, N., Avital, G., Klochendler, A., de Leeuw, Y., Anavy, L., Gennert, D., Li, S., Livak, K.J., Rozenblatt-Rosen, O., et al. (2016). CEL-Seq2: sensitive highly-multiplexed single-cell RNA-Seq. Genome Biol. *17*, 77.

Horn, T., Sandmann, T., Fischer, B., Axelsson, E., Huber, W., and Boutros, M. (2011). Mapping of signaling networks through synthetic genetic interaction analysis by RNAi. Nat. Methods *8*, 341–346.

Katz, Y., Wang, E.T., Airoldi, E.M., and Burge, C.B. (2010). Analysis and design of RNA sequencing experiments for identifying isoform regulation. Nat. Methods *7*, 1009–1015.

Kohtz, J.D., Jamison, S.F., Will, C.L., Zuo, P., Lührmann, R., Garcia-Blanco, M.A., and Manley, J.L. (1994). Protein-protein interactions and 5′-splice-site recognition in mammalian mRNA precursors. Nature *368*, 119–124.

Kolev, V., Mandinova, A., Guinea-Viniegra, J., Hu, B., Lefort, K., Lambertini, C., Neel, V., Dummer, R., Wagner, E.F., and Dotto, G.P. (2008). EGFR signalling as a negative regulator of Notch1 gene transcription and function in proliferating keratinocytes and cancer. Nat. Cell Biol. *10*, 902–911.

Kouwenhoven, E.N., Oti, M., Niehues, H., van Heeringen, S.J., Schalkwijk, J., Stunnenberg, H.G., van Bokhoven, H., and Zhou, H. (2015). Transcription factor p63 bookmarks and regulates dynamic enhancers during epidermal differentiation. EMBO Rep. *16*, 863–878.

Leclerc, E.A., Huchenq, A., Kezic, S., Serre, G., and Jonca, N. (2014). Mice deficient for the epidermal dermokine β and γ isoforms display transient cornification defects. J. Cell Sci. *127*, 2862–2872.

Levy, L., Broad, S., Diekmann, D., Evans, R.D., and Watt, F.M. (2000). Beta1 integrins regulate keratinocyte adhesion and differentiation by distinct mechanisms. Mol. Biol Cell *11*, 453–466.

Lock, F.E., Ryan, K.R., Poulter, N.S., Parsons, M., and Hotchin, N.A. (2012). Differential regulation of adhesion complex turnover by ROCK1 and ROCK2. PloS One *7*, e31423.

Mani, R., St Onge, R.P., Hartman, J.L., 4th, Giaever, G., and Roth, F.P. (2008). Defining genetic interaction. Proc. Natl. Acad. Sci. USA *105*, 3461–3466.

Marthaler, A.M., Podgorska, M., Feld, P., Fingerle, A., Knerr-Rupp, K., Grässer, F., Smola, H., Roemer, K., Ebert, E., Kim, Y.J., et al. (2017). Identification of C/EBPα as a novel target of the HPV8 E6 protein regulating miR-203 in human keratinocytes. PLoS Pathog. *13*, e1006406.

Mehic, D., Bakiri, L., Ghannadan, M., Wagner, E.F., and Tschachler, E. (2005). Fos and jun proteins are specifically expressed during differentiation of human keratinocytes. J. Invest. Dermatol. *124*, 212–220.

Michael, M., Begum, R., Fong, K., Pourreyrone, C., South, A.P., McGrath, J.A., and Parsons, M. (2014). BPAG1-e restricts keratinocyte migration through control of adhesion stability. J. Invest. Dermatol. *134*, 773–782.

Miyai, M., Hamada, M., Moriguchi, T., Hiruma, J., Kamitani-Kawamoto, A., Watanabe, H., Hara-Chikuma, M., Takahashi, K., Takahashi, S., and Kataoka, K. (2016). Transcription factor MafB coordinates epidermal keratinocyte differentiation. J. Invest. Dermatol. *136*, 1848–1857.

Moreno-Layseca, P., and Streuli, C.H. (2014). Signalling pathways linking integrins with cell cycle progression. Matrix Biol. *34*, 144–153.

Mulder, K.W., Wang, X., Escriu, C., Ito, Y., Schwarz, R.F., Gillis, J., Sirokmány, G., Donati, G., Uribe-Lewis, S., Pavlidis, P., et al. (2012). Diverse epigenetic strategies interact to control epidermal differentiation. Nat. Cell Biol. *14*, 753–763.

Nagarajan, P., Chin, S.S., Wang, D., Liu, S., Sinha, S., and Garrett-Sinha, L.A. (2010). Ets1 blocks terminal differentiation of keratinocytes and induces expression of matrix metalloproteases and innate immune mediators. J. Cell Sci. *123*, 3566–3575.

Naso, M.F., Liang, B., Huang, C.C., Song, X.Y., Shahied-Arruda, L., Belkowski, S.M., D'Andrea, M.R., Polkovitch, D.A., Lawrence, D.R., Griswold, D.E., et al. (2007). Dermokine: an extensively differentially spliced gene expressed in epithelial cells. J. Invest. Dermatol. *127*, 1622–1631.

Plaschka, C., Lin, P.-C., and Nagai, K. (2017). Structure of a pre-catalytic spliceosome. Nature *546*, 617–621.

Rappsilber, J., Mann, M., and Ishihama, Y. (2007). Protocol for micro-purification, enrichment, pre-fractionation and storage of peptides for proteomics using StageTips. Nat. Protoc. *2*, 1896–1906.

Roguev, A., Talbot, D., Negri, G.L., Shales, M., Cagney, G., Bandyopadhyay, S., Panning, B., and Krogan, N.J. (2013). Quantitative genetic-interaction mapping in mammalian cells. Nat. Methods *10*, 432–437.

Ruhrberg, C., Hajibagheri, M.A., Parry, D.A., and Watt, F.M. (1997). Periplakin, a novel component of cornified envelopes and desmosomes that belongs to the plakin family and forms complexes with envoplakin. J Cell Biol. *139*, 1835–1849.

Sen, G.L., Reuter, J.A., Webster, D.E., Zhu, L., and Khavari, P.A. (2010). DNMT1 maintains progenitor function in self-renewing somatic tissue. Nature *463*, 563–567.

Smits, A.H., Jansen, P.W., Poser, I., Hyman, A.A., and Vermeulen, M. (2013). Stoichiometry of chromatin-associated protein complexes revealed by label-free quantitative mass spectrometry-based proteomics. Nucleic Acids Res. *41*, e28.

Spartz, A.K., Herman, R.K., and Shaw, J.E. (2004). SMU-2 and SMU-1, Caenorhabditis elegans homologs of mammalian spliceosome-associated proteins RED and fSAP57, work together to affect splice site choice. Mol. Cell. Biol. *24*, 6811–6823.

Stoll, S.W., Stuart, P.E., Swindell, W.R., Tsoi, L.C., Li, B., Gandarillas, A., Lambert, S., Johnston, A., Nair, R.P., and Elder, J.T. (2016). The EGF receptor ligand amphiregulin controls cell division via FoxM1. Oncogene *35*, 2075–2086.

Tsuji, G., Ito, T., Chiba, T., Mitoma, C., Nakahara, T., Uchi, H., and Furue, M. (2018). The role of the OVOL1-OVOL2 axis in normal and diseased human skin. J. Dermatol. Sci. *90*, 227–231.

Truong, A.B., Kretz, M., Ridky, T.W., Kimmel, R., and Khavari, P.A. (2006). p63 regulates proliferation and differentiation of developmentally mature keratinocytes. Genes Dev. *20*, 3185–3197.

Tribioli, C., Robledo, R.F., and Lufkin, T. (2002). The murine fork head gene Foxn2 is expressed in craniofacial, limb, CNS and somitic tissues during embryogenesis. Mech. Dev. *118*, 161–163.

Ulrich, A.K.C., and Wahl, M.C. (2017). Human MFAP1 is a cryptic ortholog of the Saccharomyces cerevisiae Spp381 splicing factor. BMC Evol. Biol. *17*, 91.

van Buggenum, J.A.G., Gerlach, J.P., Tanis, S.E.J., Hogeweg, M., Jansen, P.W.T.C., Middelwijk, J., van der Steen, R., Vermeulen, M., Stunnenberg, H.G., Albers, C.A., and Mulder, K.W. (2018). Immuno-detection by sequencing enables large-scale high-dimensional phenotyping in cells. Nat. Commun. *9*, 2384.

van den Bogaard, E.H., Podolsky, M.A., Smits, J.P., Cui, X., John, C., Gowda, K., Desai, D., Amin, S.G., Schalkwijk, J., Perdew, G.H., and Glick, A.B. (2015). Genetic and pharmacological analysis identifies a physiological role for the AHR in epidermal differentiation. J. Invest. Dermatol. *135*, 1320–1328.

Wang, X., Castro, M.A., Mulder, K.W., and Markowetz, F. (2012). Posterior association networks and functional modules inferred from rich phenotypes of gene perturbations. PLoS Comput. Biol. *8*, e1002566.

STAR★METHODS

KEY RESOURCES TABLE

REAGENT or RESOURCE	SOURCE	IDENTIFIER
Antibodies		
Anti-ZMAT2	DSHB	PRCP-ZMAT2-1E5
Anti-Collagen type VII	MerckMillipore	MAB1345; RRID: AB_11210494
Anti-Keratin 1	BioLegend	Poly19052; RRID: AB_2565047
Anti-Ki67	Thermo Fisher Scientific	RM-9106-S0; RRID: AB_2341197
Anti-Hoechst 33342	Thermo Fisher Scientific	H1399
Anti-TGM1	Gift from R.Rice	BC.1
DRAQ5	Biostatus	DR05500
Biological Samples		
Pooled human foreskin keratinocytes	Lonza	00192906
Pooled human foreskin keratinocytes (3D culture)	PromoCell	C-12005
Chemicals, Peptides, and Recombinant Proteins		
AG1478	Calbiochem	658552
BMP 2/7	R&D systems	3229-BM-010
EGF	GIBCO	17005042
Bovine pituitary extract	GIBCO	17005042
Mitomycin C	Santa Cruz Biotechnology	sc-3514
Critical Commercial Assays		
Kapa RNA Hyperprep Kit with RiboErase	Illumina	KR1351
Amaxa SF cell line 96 well Nucleofector Kit	Lonza	V4SC-2960
Deposited Data		
Induction of differentiation Human Epidermal Stem cells (48 hours)	This paper	GEO: GSE117562
Splicing and epigenetic factors jointly regulate epidermal differentiation (5 days)	This paper	GEO: GSE114529
Experimental Models: Cell Lines		
Mouse: J2-3T3 (gift from Prof. Fiona Watt)	Derived from lab Howard Green	N/A
Oligonucleotides		
siRNAs see Table S1	Ambion	N/A
Primers see Table S1	This paper	N/A
Software and Algorithms		
STAR	Dobin et al., 2013	RRID:SCR_015899; https://github.com/alexdobin/STAR
DEXseq	Anders et al., 2012	RRID:SCR_012823; https://doi.org/10.18129/B9.bioc.DEXSeq
DESeq2	Hashimshony et al., 2016	RRID:SCR_015687; https://doi.org/10.1186/s13059-014-0550-8
MISO	Katz et al., 2010	RRID:SCR_003124; https://miso.readthedocs.io/en/fastmiso/
RedeR	Castro et al., 2012	10.1186/gb-2012-13-4-r29
MaxQuant version 1.5.1.0	Cox and Mann, 2008	RRID: SCR_014485

CONTACT FOR REAGENTS AND RESOURCE SHARING

Further information and requests for resources and reagents should be directed to and will be fulfilled by the Lead Contact, Dr. Klaas W. Mulder (k.mulder@science.ru.nl)

EXPERIMENTAL MODEL AND SUBJECT DETAILS

Primary human foreskin keratinocytes were obtained from Lonza (00192906). They were cultured on a mitotically inactivated J2-3T3 layer as described previously (Mulder et al., 2012). Prior and during experiments where differentiation was induced, the cells were grown on keratinocyte serum-free medium (KSFM, GIBCO) supplemented with 0.2 ng/mL epidermal growth factor (EGF, GIBCO) and 30 ug/mL bovine pituitary extract (BPE, GIBCO). Differentiation was induced using 10 μM AG1478 (Calbiochem), 200 ng/mL human recombinant BMP 2/7 (R&D systems) a combination of these or 10% fetal bovine serum (MP Bio) was added to the KSFM for 48 hours.

For colony formation assays, J2-3T3 cells were seeded at 100.000 cells per well in a 6 well format and inactivated using mitomycin C (2 μg/mL, Santa Cruz Biotechnology) as described previously (Mulder et al., 2012). Transfected keratinocytes (500 cells) were seeded on top and grown for 2 weeks before fixation and immunostaining.

For 3D cultures, pooled primary human foreskin keratinocytes from different donors were obtained from PromoCell and grown in a 1:1 mixture of KSF-M (GIBCO) and Medium 154 for keratinocytes (GIBCO), supplemented with Human Keratinocyte Growth Supplement, epidermal growth factor, bovine pituitary extract and 1x Antibiotic-Antimycotic (all supplements from GIBCO).

METHOD DETAILS

siRNA nucleofection

Passage 3 lip or foreskin keratinocytes were grown to 70% confluency in KSFM before they were used for nucleofection using the Amaxa system (Lonza). The cells were collected and resuspended in cell line buffer SF at 2*10ˆ5 cells per 18 uL, mixed with 2 uM siRNA. After transfection using program FF113, the cells were incubated for 10 minutes at room temperature. Finally, the transfected cells were resuspended in pre-warmed KSFM and dispensed over the culture plates manually.

For 3D culture transfection, 6 million primary human keratinocytes were electroporated with 1 nmol annealed siRNAs, using the Amaxa human keratinocyte Nucleofector kit (Lonza) according to the manufacturer's instructions and the program T-018 of the Amaxa Nucleofector II device. After nucleofection, cells were let to recover for 12-24 hr in KSFM.

siRNA library

145 genes were selected based on differential expression and RPKM over 5 in a dataset published in Kouwenhoven et al., 2015. Additionally, literature was manually searched to select those factors that had DNA binding capacities. A custom silencer select siRNA library was obtained from Ambion including 3 siRNAs per gene divided over 2 plates. The siRNA screens were performed using the pooled siRNAs per gene.

Information about individual siRNAs is included in Table S1.

siRNA screening and data processing

Passage 3 foreskin keratinocytes were grown up to 70% confluency in KFSM for nucleofection. In addition to the custom library, siRNA controls were transfected; scramble siRNAs and siRNAs targeting TGM1. After transfection, the cells were manually dispensed onto 20 96-well plates, generating quadruplicate plates for each differentiation inducing treatment plus control. The medium was refreshed the next day and after 72 hours and differentiation was induced (vehicle, AG1478, BMP 2/7, AG1478 + BMP 2/7 and serum) for 48 hours. The cells were fixed using 4% paraformaldehyde in PBS (10 minutes, at RT) and subsequently permeabilised using 0.1% Triton X-100 in PBS (10 minutes, at RT). The cells were blocked using 10% serum in PBS for 30 minutes at room temperature and subsequently stained with primary antibody targeting TGM1 (mouse anti-BC-1, 1:2000) for 1 hour at room temperature. Following 3 washes the cells were stained with mouse secondary antibody IR800 (IRDye 800CW, 1:2000) and DNA staining agent DRAQ5 (Biostatus, 1:4000) in blocking buffer for 1 hour at room temperature. After three washes a final volume of 100 uL PBS was added and the plates were scanned using the Li-Cor Odyssey CLx system. The same settings were used for each screen.

Signals were quantified using the Li-Cor Odyssey CLx software and used for subsequent analysis. The signal was normalized using the DRAQ5 DNA stain and the background signal measured in the TGM1 KD samples was subtracted. The data was further processed to z-scores based on knockdown readouts only, transforming the data to a standardized format enabling compilation of all the experimental data.

Bayesian mixture model and network visualization

The phenotypic profiles extracted from the screen, describing the effect of knockdown of a certain gene on TGM1 expression in 5 different conditions, are compared in this model. The network is visualized using the R-package RedeR (Castro et al., 2012). The Bayesian mixture model is described in Wang et al. (2012). In short, we extracted the phenotypic profiles per gene from the z-score matrix, for which the cosine correlation between each gene pair was calculated. Under the assumption that there were three possible modes of functional association; positive, negative or a lack of association, there are three beta distributions in this model. To estimate the parameters α and β for the positive and negative distribution, maximum *a posteriori* probability (MAP) inference was applied with an uninformative prior (uniform Dirichlet priors) using an expectation maximization (EM) algorithm. For the parameters of the lack of association distribution, the dataset is permutated 100 times to create a random dataset. The data is fitted to these

distributions, generating a matrix with probabilities for each gene pair belonging to one of the three distributions. This matrix is subjected to network inference, looking at functional interactions and their signal to noise ratio (SNR: probability positive or negative association/probability lack of association). We only considered functional interactions that have a SNR of 10 or higher and checked the significance of the inferred connections with multiscale bootstrap resampling. Using the approximately unbiased method (sample size between 0.5 to 1.4), we avoided a bootstrap resampling bias. The displayed p values are defined as 1-AU.

Identification genetic interactions

Cells were transfected with 2 independent siRNAs per gene and the different combinations of these siRNAs in triplicate. RNA was isolated and CEL-seq 2 libraries were prepared. After sequencing and subsequent mapping using STAR ((Dobin et al., 2013) RRID:SCR_015899) the data was analyzed using DESeq 2.0 ((Hashimshony et al., 2016) RRID:SCR_015687) to call differentially expressed genes versus siControl. We included all genes that were detected in at least 90% of the samples and significantly differentially expressed with p value < 0.05 in at least one comparison. Furthermore, samples in which more than 10% of these genes was not detected were excluded from further analysis to increase the robustness of the statistical analyses. For the remaining samples and genes, we calculated the fold change (FC) in expression compared to siControl (observed FC). The expected fold changes (NULL hypothesis in the absence of a functional interaction) were calculated using the product rule (Mani et al., 2008) multiplying the FC (equivalent to summing the log FC) for the individual knockdown samples for ZMAT2 versus the other genes. To estimate the variation of the NULL hypothesis, we performed this calculation for all combinations of independent siRNAs and replicates. The expected FC was then compared to the observed FC using a multiple testing corrected two-sided t test (Benjamini-Hochberg, FDR < 0.01). Interactions were labeled alleviating when the expected FC was higher than the observed FC and aggravating when the expected FC was lower than the observed FC.

RNA extraction, RT-qPCR and expression profiling

RNA was isolated using the Quick-RNA^{TM} MicroPrep kit from Zymo Research and subsequently 1 μg RNA was converted to complementary DNA. Thermo Maxima Reverse Transcriptase was used for reverse transcription and the resulting cDNA was diluted to ~5pmol/μL for qPCR using SYBR Green Master mix. Data was normalized using 18 s signal as a control, which was included on each plate.

For the samples generated for 3D organotypic cultures, total RNA from organotypic skin cultures was isolated using the RNeasy Plus mini kit (QIAGEN) according to the manufacturer's instructions. 1 μg total RNA was subjected to reverse transcription with the iScript cDNA synthesis kit (Biorad). For qRT–PCR measurements, the Takyon Mix (Eurogentec) was used with the CFX96 Touch Real-Time PCR Detection System (Biorad). Samples were run at least in duplicates and normalized to ribosomal protein L32 mRNA.

Primer sequences are included in Table S1.

Colony formation assay analysis

The cells were blocked using 10% serum in PBS for 30 minutes at room temperature and subsequently stained DNA staining DRAQ5 (Biostatus, 1:4000) in blocking buffer for 1 hour at room temperature. After three washes a final volume of PBS was added and the plates were scanned using the Li-Cor Odyssey CLx system. The images were processed as described in (van Buggenum et al., 2018)

Organotypic human epidermal tissue

For the generation of organotypic human epidermal tissue, 500,000 human keratinocytes that have been nucleofected with siRNAs were seeded onto a devitalized dermal matrix and raised to the air–liquid interface to initiate stratification and differentiation, as described previously (Truong et al., 2006; Sen et al., 2010). Cultures were harvested after four days. Half of the tissue was used for RNA isolation and the other half for cryosectioning.

Immunofluorescence and tissue analysis

Seven micrometer thick cross sections of human organotypic skin cultures were fixed in either 100% acetone or methanol for 10 min at −20°C followed by blocking in PBS with 10% bovine calf serum (BCS) for 20 min at RT. Antibodies were diluted in PBS with 1% BCS and incubated with the sections for one hour or overnight. The following primary antibodies were used: collagen type VII (MerckMillipore, MAB1345) at 1:800 dilution, keratin 1 (BioLegend, Poly19052) at 1:300 dilution, and Ki67 (Thermo Fisher Scientific, RM-9106-S0) at 1:100 dilution. Alexa-555-conjugated goat anti-mouse and goat anti-rabbit IgG (Molecular Probes, 1:300 dilution), and Alexa 488-conjugated goat anti-rabbit and goat anti-mouse IgG (Molecular Probes, 1:300 dilution) were used as secondary antibodies. Unbound antibodies were washed off with PBS (3 times, 5 min, RT) and nuclei were stained with 4mg/L Hoechst 33342 (ThermoFisherScientific, H1399) in PBS. Finally, slides were mounted in ProLong Gold antifade Mountant (ThermoFisherScientific) and analyzed with an Axiovert 200M fluorescence microscope and the AxioVision Software (Carl Zeiss).

IP followed by quantitative mass spectrometry

Passage 3 foreskin keratinocytes were grown up to 70% confluency in KFSM before harvesting and counting. Nuclear extracts were prepared by adding 5 volumes of buffer A (10 mM HEPES KOH pH 7.9, 1.5 mM $MgCl_2$, 10 mM KCl) and incubation of 1 hour on ice. The cells were centrifuged for 5 minutes at 450 g before lysis by dounce homogenization in 2 volumes cell pellet buffer A with 0,5%

NP40 and protease inhibitors. Cytoplasmic and nuclear extract were separated by centrifugation at 3200 g for 15 minutes and collection of cytoplasmic fraction as supernatant. The nuclear pellet was washed with 10 volume PBS and centrifuged at 3200 g for 5 minutes. Nuclei were resuspended in 2 volumes extraction buffer C (420 mM NaCl, 20 mM HEPES KOH pH 7.9, 20% v/v glycerol, 2 mM $MgCl_2$, 0.2 mM EDTA, 0.5% NP40, 0.5 mM DTT, protease inhibitors) and incubated 2 hours rotating at 4°C. The extract was centrifuged for 30 minutes at 14.000 rpm and the nuclear extract was collected. Protein concentration was determined using a Bradford assay.

500 ug nuclear extract was used in an overnight IP with 3 μg α-ZMAT2 (DSHB, RRID:SCR_013527, PRCP-ZMAT2-1E5) in a total volume of 500 μL. PCRP-ZMAT2-1E5 was deposited to the DSHB by Protein Capture Reagents Program, produced by JHU/CDI (DSHB Hybridoma Product PCRP-ZMAT2-1E5). This was mixed with 25 μL Dynabeads magnetic beads (Invitrogen) and incubated for 4 hours rotating at 4°C. After incubation, beads where washed three times using buffer A, two times using PBS, once using ABC buffer (25 mM ammonium bicarbonate) before final resuspension in 50 μL ABC buffer. Overnight digestion was performed using 350 ng trypsin where after samples were desalted using C18 stagetips (Rappsilber et al., 2007).

The tryptic peptides were separated in a 120 minute acetonitrile gradient (7% to 32%, stepwise increase up to 95%) on an Easy nLC 1000 (Thermo Scientific) connected online to a Orbitrap Fusion Tribrid mass spectrometer. Mass spectrometry and mass spectrometry/mass spectrometry spectra were recorded as described in van Buggenum et al., 2018. Data analysis was performed as described before (Smits et al., 2013) using MaxQuant version 1.5.1.0 (RRID: SCR_014485) (Cox and Mann, 2008) and protein database UniProt_201512＼HUMAN. In brief, data was analyzed using default settings of the MaxQuant software package, where after Perseus was used to filter out reverse hits and to impute missing values. Plots were made in R.

IP-RNA sample preparation

Passage 3 foreskin keratinocytes were grown up to 70% confluency in KFSM before harvesting and counting. After preparing the nuclear extract and determining the protein concentration by Bradford assay, the extract was divided over samples for input RNA isolation and IP in triplicate. For input RNA, RNA was isolated directly from the nuclear extract and stored at −20°C. IP was performed as described in the IP-mass spectrometry paragraph up to washing the beads. RNA lysis buffer was added to the beads and incubated for 5 minutes before removing the beads from the sample using the magnetic tray. RNA was isolated from the supernatant as indicated in the protocol provided with the Quick-RNA™ MicroPrep kit (Zymo Research). The isolated RNA was further processed for sequencing using the CEL-seq 2 library prepation protocol and subsequent analysis.

Epifluorescence localization ZMAT2

Cells were transfected with scramble siRNAs or siRNAs targeting ZMAT2 seeded in 96-well glass bottom plates and cultured for 72 hours as indicated. Cells were washed, fixed using 4% paraformaldehyde for 10 minutes and subsequently permeabilised using 0.3% triton in PBS for 10 minutes. The cells were pre-blocked using 0.2M glycine for 20 minutes and blocked for 1 hour using 1% BSA. Cells were incubated overnight at 4°C with primary stain, which included a no-primary-antibody control and 4 μg/mL α-ZMAT2 (DSHB, PRCP-ZMAT2-1E5). After three wash steps with PBS cells were stained with secondary antibody Alexa 488 rabbit α-mouse (1:2000) for 1 hour and DAPI (1:500) in the last 10 minutes. Cells were washed 3 times and imaged on a Leica DMI6000B automated high-content microscope.

Library preparation RNA sequencing

RNA sequencing libraries were prepared as described in the protocol supplied with the Illumina KAPA RNA HyperPrep Kit with RiboErase (HMR) – (KR1351), starting from 500 ng. The concentration of the libraries was determined using the Denovix HS dsDNA assay and library quality was checked using the Bioanalyser platform (Agilent). Samples were sequenced using the NextSeq500 (Illumina) platform.

CEL-seq 2

CEL-seq 2 libraries were generated using the protocol from (Hashimshony et al., 2016) with the following adaptations. 100pg purified RNA was directly added to a reverse transcription mixture containing Maxima H Minus (ThermoFisher) reverse transcriptase and CEL-seq 2 primers with a 6-nucleotide sample barcode and 8-nucleodide UMI. After reverse transcription samples were pooled and purified using AmpureXP beads (Beckman Coulter). Second strand synthesis was performed according to the original protocol, libraries were amplified using 2 consecutive PCR reactions.

Data analysis sequencing data

CEL-seq 2 data was processed using the Yanai pipeline (Hashimshony et al., 2016) up to count tables which were further processed using DESeq 2.0. RNA sequencing data from KAPA RNA HyperPrep kit generated libraries was aligned (hg38, annotation: ensembl genecode basic annotation V27) and sorted using STAR and analyzed using DEXSeq ((Anders et al., 2012) RRID:SCR_012823). For the analysis using MISO ((Katz et al., 2010) RRID:SCR_003124) the sequencing data was aligned to hg19 using STAR where after the collection annotations under the Human genome (hg19) alternative events v1.0 was used to call alternative events. Data regarding the siRNA knockdown of ZMAT2 and SRSF1 is deposited in GEO (RRID:SCR_005012) under accession code GSE114529, and data regarding the induction of differentiation is deposited under accession code GSE117562.

Expression ZMAT2 in different tissues

Expression of ZMAT2 and other spliceosome components was taken from the EMBL expression atlas, which extracts its raw data from the PRIDE proteomics database. Website open source database: https://www.ebi.ac.uk/gxa/home/

FACS analysis

Viability, apoptosis and cell cycle state were analyzed using the MUSE Cell Analyzer (EMD Millipore). Cells were counted and subsequently stained using MUSE Count and Viability Reagent (EMD Millipore) as indicated in the protocol for 5 minutes. In parallel, cells were stained using annexinV-PE (BD, 1:25 in PBS) for 15 minutes before analysis on the MUSE Cell Analyzer (EMD Millipore). Pre-programmed software allowed easy setting of the gates in the Count and Viability protocol and the AnnexinV and Cell Death protocol. For cell cycle analysis, cells were counted, fixed using 70% ethanol overnight at −20°C and stained using 50 μg/mL propidium iodide, 100 ug/mL RNase A, 0,1% Triton and 0,1% BSA in PBS for 1 hours at room temperature. Pre-programmed software was used to set the gate in the Cell Cycle Assay protocol.

QUANTIFICATION AND STATISTICAL ANALYSIS

Quantification and statistical analysis was performed as described in the sections describing the applied techniques. Statistical tests and parameters were performed as reported in the appropriate figure legends and sections of the manuscript.

DATA AND SOFTWARE AVAILABILITY

Data resources

The accession numbers for the RNA sequencing data reported in this paper are GEO (RRID:SCR_005012): GSE114529 (siRNA knockdown of ZMAT2 and SRSF1) and GSE117562 (induction of differentiation). The data that was generated in the siRNA screen and subsequent processing steps can be found in Data S1.